Combustion and Flame 162 (2015) 3449–3455

Contents lists available at ScienceDirect

Combustion and Flame

journal homepage: www.elsevier.com/locate/combustflame

Emulation of condensed fuel flames with gases in microgravity

Yi Zhang[a], Matt Kim[a], Haiqing Guo[a], Peter B. Sunderland[a], James G. Quintiere[a,*], John deRis[b,1], Dennis P. Stocker[c]

[a] Dept. of Fire Protection Engineering, University of Maryland, College Park, MD 20742, USA
[b] FM Global, USA
[c] NASA Glenn Research Center, USA

ARTICLE INFO

Article history:
Received 28 March 2015
Revised 4 May 2015
Accepted 5 May 2015
Available online 10 June 2015

Keywords:
Diffusion flame
Fire
Heat flux
Microgravity

ABSTRACT

A gaseous fuel burner has been designed to emulate the burning behavior of liquids and solids. The burner is hypothesized to represent a liquid or solid fuel through four key properties: heat of combustion, heat of gasification, vaporization temperature, and laminar smoke point. Previous work supports this concept, and it has been demonstrated for four real fuels. The technique is applied to flames during 5 s of microgravity. Tests were conducted with a burner of 25 mm diameter, two gaseous fuels, and a range of flow rates, oxygen concentrations, and pressures. The microgravity tests reveal a condition appearing to approach a steady state but sometimes with apparent local extinction. The flame typically retains a hemispherical shape, with some indication of slowing growth, and nearly asymptotic steady flame heat flux. A one-dimensional steady-state theory reasonably correlates the data for flame heat flux and flame length. The burning rate per unit area is found to be inversely dependent on diameter and a function of the ratio of the ambient oxygen mass fraction to the heat of gasification. The flame length to diameter ratio depends on two dimensionless parameters: Spalding B number and the ratio of the heat of combustion per unit mass of ambient oxygen to the heat of combustion of the fuel mixture stream.

1. Introduction

It is hypothesized here that the burning of condensed fuels can be emulated with a gaseous fuel burner that matches four key properties. The gas burner is called the Burning Rate Emulator (BRE). These properties are: heat of combustion, surface temperature, smoke point (SP), and heat of gasification. Heat of combustion is related to flame shape and therefore both convective and radiative heat flux. Surface temperature is related to the boiling point of liquids and the pyrolysis temperature of solids. Smoke point is related to the flame radiative emissions. Heat of gasification is related to the heat required to vaporize or pyrolyze the fuel.

On Earth, gravity enhances most fires by entraining air. Nevertheless, most solids and many liquids require external heating to sustain burning. It is more difficult to study the burning of condensed fuels in microgravity because they are generally more likely to require external heating or flow. Accidental fires have occurred in microgravity, and microgravity experiments have identified the required conditions for spread. The state of knowledge for condensed fuel burning in microgravity was documented by Ross [1], but much remains to be learned and experimental research continues, e.g., Refs. [2–6].

Experiments in Skylab [1,7] demonstrated the sustained microgravity burning of thin paper and plastics. More recent microgravity experiments observed flame spread on thin paper and thin plastic cylinders [1]. Flame spread on 4.5 mm diameter rods of Delrin, PMMA and HDPE in the Mir space station was achieved in opposed flows down to 1 cm/s. Below 1 cm/s, the spread and burning ceased [1]. Opposed flow spread has been well documented, and is more favorable than concurrent spread. Opposed flow flame spread in quiescent microgravity has been shown to depend on material, thickness, and oxygen concentration [1].

Perhaps the most striking example of quasi-steady burning has been the burning of candle flames on the Mir [1] for up to 45 min. A hemispherical flame formed around the wick. Such experiments demonstrate quasi-steady sustained burning in quiescent microgravity. This is also born out in droplet experiments by Kumagai and others [1]. Small diameter jet flames of 0.4–2.7 mm yielded spherical flames of durations from 150 to 300 s [1]. Sunderland et al. [8] reported on microgravity jet diffusion flames for burner

* Corresponding author at: University of Maryland, Dept. of Fire Protection Engineering, 3104 J.M. Patterson Building, College Park, MD 20742, USA.
Fax: +1 (301) 405 9383.
E-mail address: jimq@umd.edu (J.G. Quintiere).
[1] Retired.

http://dx.doi.org/10.1016/j.combustflame.2015.05.005
0010-2180/

Nomenclature

B	Spalding B number, Eq. (10)
C	heat flux sensor calibration constant
c_p	specific heat
D	burner diameter
E	sensor output
f	function defined by Eq. (18)
h_B	convective heat transfer coefficient
Δh_c	heat of combustion per mass of fuel
$\Delta h_{c,ox}$	heat of combustion per mass of oxidizer
k	thermal conductivity
L	heat of gasification
$\dot{m}''$	burning rate
p	pressure
$\dot{q}''_f$	incident flame heat flux
$\dot{q}''_{f,conv}$	convective flame heat flux
$\dot{q}''_{f,r}$	radiative flame heat flux
$\dot{q}''_{net}$	net heat flux
r	radius, or stoichiometric oxygen to fuel ratio
SP	smoke point
T	temperature
X	mole fraction
y	flame height
Y	mass fraction

Greek

α	absorptivity
δ	stagnant layer thickness
ε	emissivity
σ	Stefan–Boltzmann constant

Subscripts

B	blowing effect
f	flame
F,o	fuel in supply stream
H	gauge
ox	oxidizer
$r = 0$	condition at centerline
$r = 0.825$	condition at radius of 0.825 cm
s	surface
v	vaporization
∞	ambient

diameters up to 3.3 mm that were spherical at low Reynolds numbers.

A spherical flame shape can form a stable quasi-steady flame for droplets, jets at low *Re*, and candles. Planar surfaces burning in microgravity (with weak oxidizer flow) could also remain stable with similar flame shapes. Brahmi et al. [9] used a gaseous burner to simulate burning in microgravity. They burned ethane over a 60 × 60 mm sintered bronze plate in oxygen–nitrogen atmospheres flowing over the plate at velocities of about 10–150 mm/s. Quasi-steady ellipsoidal flames were produced for this planar geometry with oxidizer velocities on the order of 5 mm/s.

NASA assesses the flammability hazard of materials for use in space flight by an upward flame spread pass-fail test STD-6001, Test 1, and supplements with data from the cone calorimeter, Test 2 [10]. Test 2 can measure three of the four properties matched by the BRE. Hence, the successful application of the BRE in microgravity can enhance the usefulness of Test 2. This would put the hazard assessment in terms of properties that control burning in microgravity. Ohlemiller [11], in evaluating the NASA tests, recommended changes to include external heat flux. In the application of the BRE, the derived heat of gasification can be regarded as an effective value composed of the material properties minus the net external heat flux divided by the burning flux. Therefore its results implicitly contain the effect of external radiation, which is so significant for burning on Earth.

A rectangular burner was developed to examine natural convection burning in normal gravity at a full range of 360° orientations. This showed good agreement with liquid fuels burning on a rectangular wick, and with theory [12].

Previous work pioneered the use of sintered metal burners for studying the steady burning of a planar condensed-phase [13–15]. They examined their results in terms of the Spalding B number for pure convection, and developed dimensionless results in accordance with theory. The B number was varied by diluting the gaseous fuel in which the heat of gasification was determined from the known flow rate of the fuel and heat flux received by the burner. Unfortunately heat flux was measured with a water-cooling array, which had a slow response time.

This study emulates the burning of condensed fuels with a gas burner. Tests are performed in microgravity and in normal gravity. The results are correlated over a wide range of conditions by a steady-state theory. The burner can be used to define the flammability domain of steady burning for a given burning configuration and ambient conditions. Although only true steady burning can be emulated, an effective overall time-average heat of gasification might be assigned to an unsteady instance, such as for a charring material. In that manner, the BRE would apply.

Operationally the burning properties we seek to match are the heat of combustion, the smoke point, the heat of gasification, and the surface temperature in steady burning. A given fuel and diluent mixture corresponds to a fuel mixture heat of combustion and smoke point. These two properties are found from known data of the pure gaseous fuel. A fuel flow rate is set and it is observed if a steady flame will occur. By measuring the heat flux and temperature, the heat of gasification and burning surface temperature are found. By varying fuel, diluent, flow rate and ambient oxygen the feasibility of steady burning can be assessed efficiently. The resulting flammability range of burning can then be related to real solid fuels with the same properties.

2. Experimental

The current BRE burner is shown in Fig. 1. This includes an inlet plenum to distribute the fuel flow, a core matrix for flow alignment, and a top plate with holes for gas flow. The uniformity of the flow is different from the vaporization of real condensed phase fuels. However, previous studies [7–10] have shown that the flame will assume a realistic position (i.e., as found in burning condensed-phase fuels) because the fuel velocity is small or comparable to the diffusion velocity. This difference in flow distribution is an implicit assumption for the burner simulation of condensed-phase fuels. The flow rate of the supply fuel stream is measured by a mass flow meter of accuracy within 10%.

The four properties required for the BRE are adjusted as follows. Heat of combustion is adjusted using dilution of a pure gaseous fuel with an inert such as nitrogen. Surface temperature is

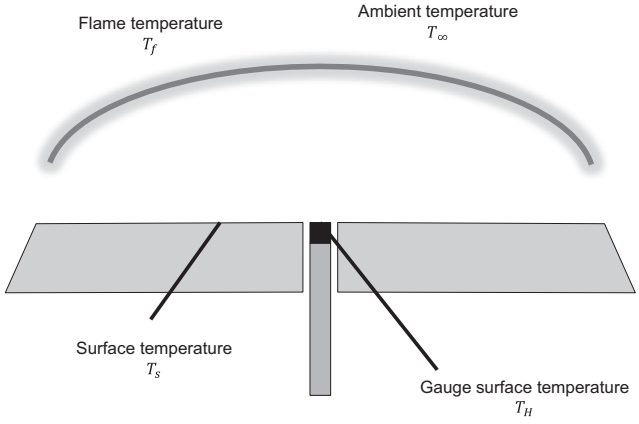

Fig. 1. Schematic of the flames.

measured by attached thermocouples, smoke point is found from the literature for the given dilution, and heat of gasification is found by appropriate averaging two heat flux sensors on the burner.

The use of the heat flux sensors requires corrections to obtain the net heat flux into the burner surface associated with the emulated condensed-phase material. For steady burning of condensed fuels, the heat of gasification, L, is related to the net heat flux as

$$\dot{q}''_{net} = \dot{m}'' L. \tag{1}$$

This equation applies locally and on average. Two sensors will give signals from which the local net flux can be derived. With an appropriate averaging of the local flux, an average value can be related to the mass flow rate of fuel of the burner. Then the value of L associated with the condensed phase fuel can be calculated.

The net heat flux (ignoring external radiant heating without any loss of generality) is composed of the incident flame radiative flux, the flame convective (or conductive for microgravity) flux, and the re-radiation flux from the surface to the ambient:

$$\dot{q}''_{net} = \alpha_s \dot{q}''_{f,r} - \varepsilon_s \sigma (T_s^4 - T_\infty^4) + h_B (T_f - T_s). \tag{2a}$$

The net flux given here is that which would occur at a specific location on the burner. This quantity cannot be found without identifying many flame characteristics. However, fast responding sensors are used to record the heat flux at two points on the burner. These sensors are thermopile heat flux transducers (Medtherm[2] models 8-1.8-10SB-4-0-36-20425AT and 4-10SB-1.4-0.43-4-36-21919T). The sensor will have its own temperature T_H, surface absorptivity, α_H, and emissivity, ε_H, all different from the burner at that same radial position. The local convective heat transfer coefficient (with mass transfer or blowing) is the same for the burner and the sensor. The sensor output measures the absorbed heat flux for the thermopile. This absorbed heat flux is given in terms of the sensor output and its recorded temperature as

$$CE = \alpha_H \dot{q}''_{f,r} + h_B (T_f - T_H) - \varepsilon_H \sigma (T_H^4 - T_\infty^4) \tag{2b}$$

where C is the calibration constant for the sensor in units of kW/m^2/mV of sensor thermopile output, and E is the output of the thermopile in mV. CE is the heat flux conducted through the material for which the thermopile measures the temperature difference. The flame temperature and incident radiative heat flux seen by the sensor are those for the same position as the sought net flux of Eq. (2a).

[2] Product references are for clarity and do not indicate an endorsement on the part of NASA or the federal government.

Now subtracting the sensor response (2b) from Eq. (2a) gives a way to obtain the net flux from CE:

$$\dot{q}''_{net} = CE + (\alpha_s - \alpha_H)\dot{q}''_{f,r} - \varepsilon_s \sigma (T_s^4 - T_\infty^4) + \varepsilon_H \sigma (T_H^4 - T_\infty^4) + h_B (T_H - T_s). \tag{3}$$

Eq. (3) can be simplified if the burner and the sensor have the same radiative properties. This was done by using the same paint for both, and calibrating the sensor with this paint. The heat flux sensors were calibrated traceable to a NIST standard. Accuracy is within 10%. The paint used here for both the sensor and the BRE top plate was Nextel Suede 3101. A pyrometer with a spectral response of 8–14 μm found this paint to have an emissivity of nearly unity and an absorptivity of 0.98. With this paint, Eq. (3) simplifies to

$$\dot{q}''_{net} = CE + \varepsilon \sigma (T_H^4 - T_s^4) + h_B (T_H - T_s). \tag{4}$$

This result still requires an estimate of the heat transfer coefficient. As this equation will be used to compute the local net flux at two radial positions, the heat transfer coefficient would need to be known at each location. This is not easily done, so an estimate will be based on its average value.

In general, a correlation giving the heat transfer coefficient for pure heat transfer is available in the literature and can then be corrected for blowing. This could have been done for the microgravity study here. Instead, an estimate was found directly from the sensor measurement. This involves an approximation of assuming purely convective heat transfer to the sensor. However, even with radiation present, its neglect is a reasonable way to make an estimate for the net heat flux from the sensor calibration. Moreover it can be shown that the departure of the corrected net heat flux from CE alone is relatively small. So this is an estimate of a small effect.

The method to estimate h_B is as follows. From *pure convection* stagnant-layer burning theory, e.g., Refs. [16–18], the convective flame heat flux is

$$\dot{q}''_{f,conv} \equiv h_B (T_f - T_s) = \dot{m}'' L = h_B [Y_{ox,\infty} \Delta h_c / c_p r - (T_H - T_\infty)]. \tag{5}$$

If there is no flame radiation, Eq. (2b), the sensor output is

$$CE = \dot{q}''_{f,conv} - \varepsilon_H \sigma (T_H^4 - T_\infty^4). \tag{6}$$

Combining Eqs. (5) and (6) yields

$$h_B = \frac{CE + \varepsilon \sigma (T_H^4 - T_\infty^4)}{Y_{ox,\infty} \Delta h_c / c_p r - (T_H - T_\infty)}. \tag{7}$$

Eqs. (4) and (7) allow the determination of the net heat flux to the BRE surface.

3. Normal gravity results

Before exploring microgravity conditions, the BRE was tested in normal gravity. Four condensed fuels were considered: methanol, heptane, polymethylmethacrylate (PMMA) and polyoxymethylene (POM). These fuels were emulated with propylene, ethylene, and methane diluted with nitrogen, as summarized in Table 1. Images of the corresponding flames for the condensed fuels and the BRE are shown in Fig. 2.

The heat of combustion is readily matched by the selection of the gaseous fuel mixture. The smoke point is approximately matched. The surface temperature is more difficult to match, as the BRE contains no controlled heating or cooling system. Therefore the equilibrium surface temperature is recorded as it results. However, as can be shown in Eq. (5), the heat loss associated with the surface temperature is small compared to the flame heat flux. So perfectly matching the surface temperature is not necessary or feasible. The key derived property that shows an

Table 1
BRE emulations of 50 mm diameter pool fires.[a]

Fuel	Methanol	BRE ($X_{CH4} = 52\%, X_{N2} = 48\%$)	Heptane	BRE (C_2H_4)	PMMA	BRE ($X_{C3H6} = 50\%, X_{N2} = 50\%$)	POM	BRE ($X_{CH4} = 41\%, X_{N2} = 59\%$)
$Y_{F,o}\,\Delta h_c$ (kJ/g)	19	19	41.2	41.5	24.2	24.3	14.4	14.1
SP (mm)	∞	∞	139	120	105	117	∞	∞
T_s (°C)	64	160	98	211	390	312	420	167
L (kJ/g)	1.2	1.24	0.4	0.51	1.6	1.8	2.4	2.1

[a] Properties are from Refs. [16,19] except that smoke points are from Ref. [20].

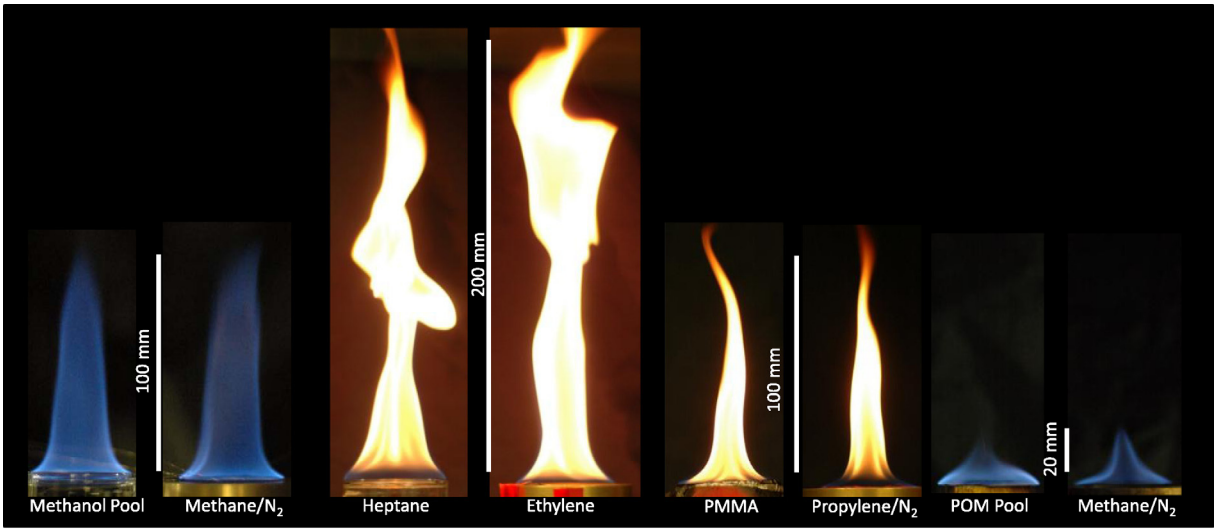

Fig. 2. Normal-gravity flames of condensed-phase fuels compared to the BRE. Details of the conditions are in Table 1. The same burning rate is used for each.

approximate match is the heat of gasification derived from the heat transfer process. Figure 2 demonstrates that the BRE can emulate the combustion of the four condensed-phase fuels in normal gravity. By matching the heat of combustion and the fuel flow rate the flame shows a similar height, color and flickering behavior. The matching of the smoke point would ensure similar flame radiation loss fractions and similar peak temperatures.

The results of Fig. 2 depend on the heat flux distribution, whereas an average net heat flux over the burner was derived from the two discrete sensors. The heat flux distribution of small pool fires (25–100 mm) have fluxes that vary considerably between the center and the edge. Akita and Yumoto [19] indicate that the heat flux increases exponentially with radius. This can be further refined in future tests. This distribution is more uniform in microgravity.

4. Microgravity results

Tests were performed in the NASA Glenn 5 s drop facility using the 25 mm BRE in a quiescent chamber. The flames were ignited approximately 1 s before the drop. It was found that ignition during the drop caused too much disturbance, so ignition before was adopted. Figure 3 suggests that, in general, the flame quickly transformed to a spherical-like microgravity flame.

Two hydrocarbon fuels were examined in microgravity: methane and ethylene. In general the methane flames appeared to be less stable and showed signs of local extinction and/or partial lifting. The conditions at the end of the test are summarized in Table 2. The flow rate, oxygen mole fraction, pressure, and fuel dilution were varied.

Figure 3 summarizes a representative microgravity test. Here the time datum is the start of the drop and the flame length is that along the burner axis. The heat flux approaches an asymptote indicative of a quasi-steady state, with the center reading slightly lower. The growth of flame length continues but appears to slow in some cases. Obviously, the tests have not reached steady-state for this short microgravity period. The assumption that the data at the end of the drop represents a nearly steady state allows the determination of L at that point from Eq. (1), as the data yield the mass flow rate and the flame heat flux. With this assumption, the data may be analyzed as if they are steady. One can then assess the credibility of the values for L in terms of condensed phase fuels. While the approach of the heat flux to a constant at the end of the test may justify this quasi-steady assumption it can be argued that the convective heat flux is trading off with the flame radiation. As the flame moves away from the surface convection drops and radiation can increase due the larger radiation path length.

As seen in Fig. 3, the flames are roughly segments of spheres, and the heat fluxes measured at the center and at about 2/3 from the center are nearly the same. Near the edge at 12.5 mm, the heat flux would be higher due to the closer proximity of the flame. Unlike for normal gravity where this heat flux distribution considerably varies, the typical microgravity results as represented in Fig. 3 show a nearly uniform heat flux over at least the first 2/3 of the burner radius. Therefore, an average heat flux was found from a weighted radial average of the two sensors. Integration leads to

$$\dot{q}''_{net} = \frac{\int_0^{1.25} 2\pi r\left[\frac{\dot{q}''_{r=0.825\ \mathrm{cm}} - \dot{q}''_{r=0\ \mathrm{cm}}}{0.825} r + \dot{q}''_{r=0\ \mathrm{cm}}\right] dr}{\pi\,(1.25)^2}$$
$$= -0.01\dot{q}''_{r=0\ \mathrm{cm}} + 1.01\dot{q}''_{r=0.825\ \mathrm{cm}}. \quad (8)$$

which is nearly uniform. Given this approximation, the nature of this heat flux can be examined for the duration of a drop test. Except for a region of soot near the top of the flames, the flames are blue and have weak local radiative losses.

Table 2 summarizes all of the microgravity tests at about 5.2 s. These tests correspond to a broad range of the four key

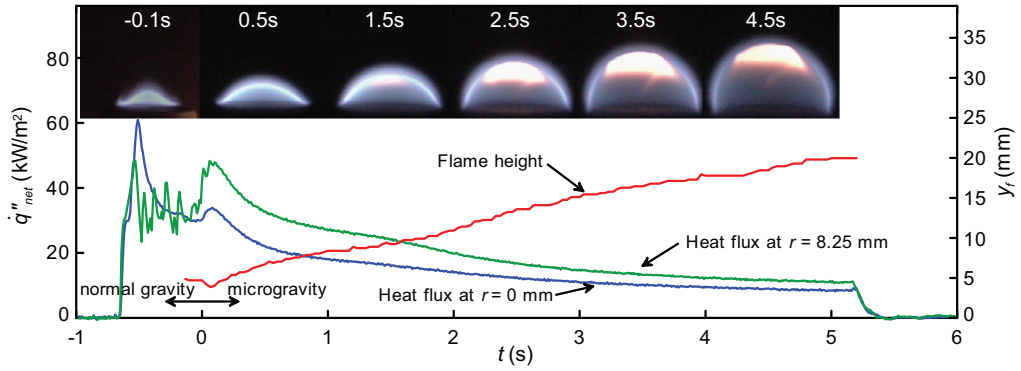

Fig. 3. A typical microgravity test, with 100% C_2H_4, 3.48 g/m^2 s, 30% O_2, and 0.7 bar.

Table 2
Microgravity drop test summary: conditions and results.

Symbol	Gas	$\dot{m}''$ [a] (g/m^2 s)	X_{O2}	p (bar)	$Y_{F,o}\,\Delta h_c$ (kJ/g)	SP mm	L [b] (kJ/g)	T_s (°C)	$\dot{q}''_{net}$ [c] (kW/m^2)	y_f [d] (mm)
○	CH_4	9.05	0.3	1	49.6	∞	0.41	31.8	3.7	NA
○	CH_4	6.67	0.3	1	49.6	∞	0.94	46.7	6.3	38
⬤	CH_4	6.67	0.21	1	49.6	∞	0.40	39.8	2.6	NA
○	CH_4	6.67	0.3	1	49.6	∞	1.43	50.1	9.6	42
○	CH_4	12.71	0.3	1	49.6	∞	0.33	45.6	4.2	NA
○	CH_4	4.72	0.3	1	49.6	∞	1.13	49.0	5.3	34
○	CH_4	12.71	0.3	1	49.6	∞	0.30	40.5	3.9	NA
○	CH_4	9.05	0.3	1	49.6	∞	0.43	39.0	3.9	NA
●	C_2H_4	6.02	0.21	1	41.5	120	0.65	35.2	3.9	36
●	C_2H_4	6.02	0.21	1	41.5	120	0.67	31.4	4.0	37
●	C_2H_4	4.63	0.21	1	41.5	120	1.28	36.8	5.9	34
●	C_2H_4	3.48	0.21	1	41.5	120	2.24	30.2	7.8	23
▩	C_2H_4	3.48	0.3	1	41.5	NA	3.94	37.8	13.7	15
■	C_2H_4	3.48	0.3	0.7	41.5	NA	3.17	38.2	11.0	19
▲	C_2H_4	3.48	0.26	0.81	41.5	NA	2.37	33.2	8.2	20
△	C_2H_4	3.48	0.26	1	41.5	NA	2.99	35.5	10.4	18
□	C_2H_4	3.48	0.3	0.5	41.5	NA	2.57	34.9	8.9	NA
□	C_2H_4	3.48	0.3	0.5	41.5	NA	2.23	34.5	7.8	25
♦	50% C_2H_4	6.95	0.21	1	20.8	240	0.62	29.5	4.3	35
◇	50% C_2H_4	6.95	0.26	1	20.8	NA	0.86	35.4	5.9	NA
◇	50% C_2H_4	6.95	0.26	1	20.8	NA	0.90	35.8	6.3	29
◊	50% C_2H_4	6.95	0.26	0.81	20.8	NA	0.69	32.8	4.8	34
♦	50% C_2H_4	9.26	0.21	1	20.8	240	0.41	29.4	3.8	45
◊	50% C_2H_4	9.26	0.26	0.81	20.8	NA	0.54	35.0	5.0	39

[a] Including fuel and diluent.
[b] From Eq. (1).
[c] From Eqs. (4) and (7).
[d] The maximum distance between the flame and the burner surface at the end of the drop.

properties. The *heat of combustion* of the supply fuel stream and the *smoke point* (where available) are determinable for each fuel mixture. The *surface temperature* of the burner is measured and averaged, and the *derived L value* is computed. For a condensed fuel having these properties, the burn rate per unit area is measured and the flame shape recorded. The values in Table 2 of the fuel mixture stream heat of combustion and heat of gasification correspond to typical liquid fuels and some plastics. This can be seen from representative values as shown in Table 1. Although the microgravity flames are still slowly changing in size and cannot be taken as steady, the derived heat of gasification corresponds to a steady burning condition for a surrogate condensed-phase fuel. If such condensed-phase fuels exist that have the properties of Table 2, the results suggest that they would burn steadily in microgravity. Of course, the final proof of this is a longer period test with steady conditions attained.

The results in Table 2 allow the generation a *flammability map* that potentially shows what properties permit steady burning to occur in microgravity. Burning rate is a function of the key four material properties and environmental conditions. Empirically the mass flux at burning is plotted against the heat of gasification in Fig. 4 where only discriminating attention is paid to the ambient oxygen concentration. The range of L values correspond to liquid and some plastic fuels. Heat of combustion of the supply fuel mixture stream, smoke point, surface temperature, and pressure are not distinguished in the plot. Essentially this says that heat of combustion varying from about 20 to 50 kJ/g, SP > 100 mm, surface temperatures between about 30 and 50 °C, and pressures of 0.5–1 atm have negligible influence on the plot. The mass flux for these conditions is primarily a function of L, with a small increase as the ambient oxygen concentration is increased.

5. Model

The microgravity tests can be represented as diffusive combustion from a circular disk into a semi-infinite medium. Here a simple approach is used to model the data at the end of the test and as represented in Table 2 and Fig. 4. Radiation is neglected and a flame-sheet model for fast chemistry is chosen. Although the flames are two dimensional, a one-dimensional analysis will

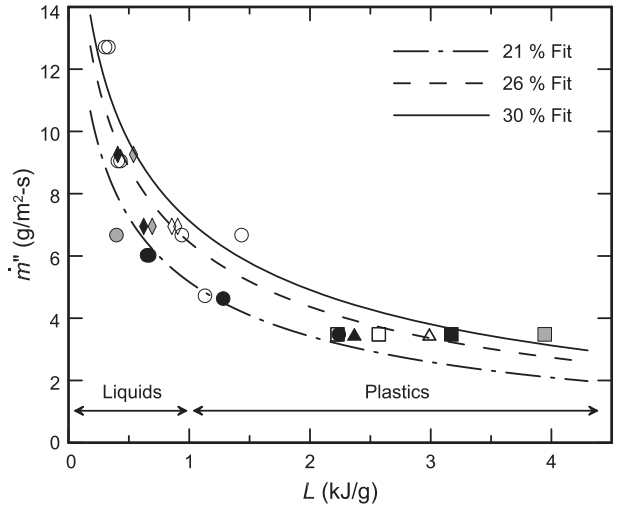

Fig. 4. The range of derived BRE L values and microgravity burning rates. The symbol legend is shown in Table 2. Typical L values for liquid and solid fuels are indicated for comparison e.g. data of Table 1. Fits are based on Eq. (16).

suffice as a first examination. In essence we are taking the data at the end of the microgravity phase (~5.2 s) to be represented as steady.

The classical one-dimensional stagnant layer model yields an exact solution for diffusive evaporative combustion across a specified layer thickness of distance, δ [16,20,21]. The results for the stagnant layer are given for the burning flux and the flame position as follows. The burning rate is

$$\dot{m}'' = \left(\frac{k}{c_p\delta}\right)\ln(1+B), \tag{9}$$

where

$$B \equiv \frac{Y_{ox,\infty}\Delta h_c/r - c_p(T_v - T_\infty)}{L}. \tag{10}$$

In this formulation, Δh_c and r pertain to the undiluted fuel in the supply stream.

The flame position is

$$\frac{y_f}{\delta} = \frac{\ln[(1+B)/(Y_{ox,\infty}/(rY_{F,o})+1)]}{\ln(1+B)}, \tag{11}$$

where $Y_{F,o}$ is the mass concentration of the fuel in the fuel/diluent mixture.

A key variable to consider is δ. For pure conduction from a circular disk in a semi-infinite medium, the average heat flux at the surface can be found as follows [22]

$$\dot{q}'' = \frac{8k}{\pi D}(T_v - T_\infty). \tag{12}$$

From Eqs. (1) and (9), the heat flux can be written as

$$\dot{m}''L = \dot{q}'' = \left(\frac{k}{c_p\delta}\right)\ln\left(1 + \frac{Y_{ox,\infty}\Delta h_c/r - c_p(T_v - T_\infty)}{L}\right)L. \tag{13}$$

Considering the case of B becoming small with no chemical reaction, Eq. (13) yields the pure conduction limit (reversing the sign for heat transfer from the disk) $\dot{q}'' = (k/\delta)(T_v - T_\infty)$. Hence δ can be identified in Eq. (9) by Eq. (12) as

$$\delta = \frac{\pi D}{8}. \tag{14}$$

However, in the interpretation of δ for the flame position in Eq. (11), it must be the value associated with blowing. Therefore the layer corresponding to combustion with mass transfer is

$$\delta_B = \delta\frac{B}{\ln(1+B)}. \tag{15}$$

This must be larger than the value for pure conduction. This blowing value is needed in Eq. (11). The actual two-dimensional case would not give a single value of y_f. So y_f in the experimental results, as shown in Table 2, must be considered at least proportional to that of Eq. (11).

From the above theoretical analysis, the average net heat flux is represented as

$$\dot{q}'' = \left(\frac{8k}{c_p\pi D}\right)\ln\left(1 + \frac{Y_{ox,\infty}\Delta h_{c,ox}}{L}\right)L, \tag{16}$$

because $T_v \approx 35$ °C for most of these tests, the temperature term in the B number is small and can be neglected. Figure 5 shows a favorable agreement between the theory and data, where the theoretical slope is given from Eq. (16) as

$$\frac{8k}{c_p\pi D} = \frac{8 \times 0.026\ \text{W/m K}}{1.04\pi \times 0.025\ \text{J m/g K}} = 2.55\ \text{g/m}^2\ \text{s}. \tag{17}$$

Here the value of thermal conductivity for air was taken at 35 °C. The linear fit of all of the data gives a slope of 3.87 compared to this theoretical value of 2.55. The ratio of the fit slope to the theory is about 1.5; this could be interpreted as a correction factor to $8/\pi$, the stagnant layer is approximate. Also the theoretical results are consistent with the empirical plot shown in Fig. 4. Three fitted curves corresponds to different oxygen concentrations, and the fitting yields slopes of 3.69 (21% O_2), 4.13 (26% O_2), and 4.27 (30% O_2), respectively. The theory shows no dependence on heat of combustion, SP, and pressure. However, radiation is not accounted for in the theory.

Now the flame length is compared to the value suggested by the theory. Eq. (15) is substituted into Eq. (11) for the blowing effect and $\frac{y_f}{D}$ is plotted vs

$$f(L, Y_{F,o}) \equiv \frac{\ln[(1+B)/(Y_{ox,\infty}/(rY_{F,o})+1)]}{\ln(1+B)}\left[\frac{B}{\ln(1+B)}\right], \tag{18}$$

where the theoretical slope is $\pi/8$. The blowing term is added here because in the theory δ must be replaced by δ_B of Eq. (15). With data from Table 2, one finds $B \approx \frac{Y_{ox,\infty}\Delta h_{c,ox}}{L}$, $r = \frac{\Delta h_c}{\Delta h_{c,ox}}$ and $Y_{F,o}$ is unity for pure fuel and 0.5 when diluted with nitrogen. (Note 50% by volume from Table 2 conforms to 0.5 by mass since C_2H_4 has the same

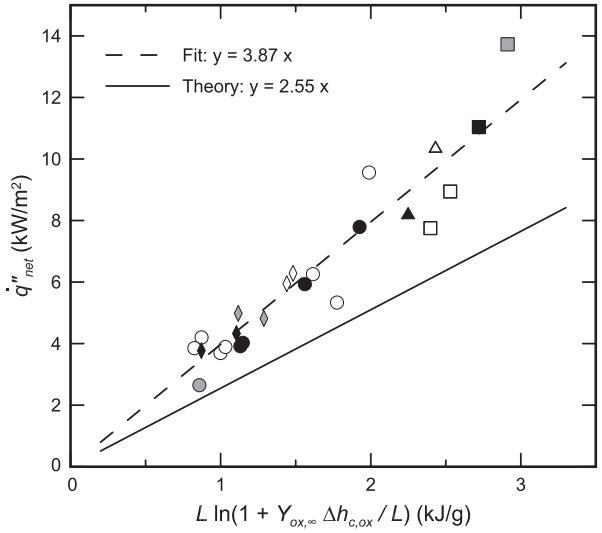

Fig. 5. Stagnant layer theoretical correlation for near steady microgravity burning. The symbol legend is shown in Table 2.

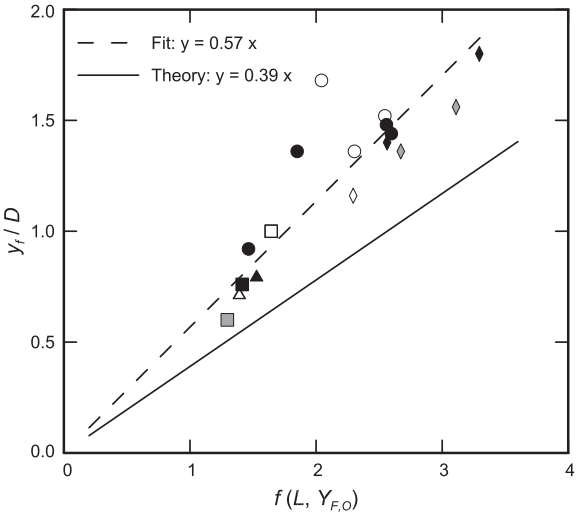

Fig. 6. A correlation for the flame length in near steady microgravity burning. The symbol legend is shown in Table 2.

molecular weight as N_2.) The plot shown in Fig. 6 again gives a reasonable correlation for the data as based on steady theory. While the theoretical slope is lower than the fitted value, their ratio also indicates that $8/\pi$ should be increased by about 1.5. This 1.5 factor must be viewed as an empirical correction to the theory for both the burning rate and the flame standoff distance. However, the size of the flame has been explained by this theory in terms of the effects of ambient oxygen, pressure and fuel L and Δh_c. Again pressure is not explicit in the theory, and therefore pressure is not expected to influence the burning rate and flame size, at least for these data at a diameter of 25 mm.

6. Conclusions

A burner has been used to emulate steady burning for condensed phase fuels. Past work has found this be an efficient way to study burning in normal gravity without burning solids or liquids. Here it is shown how the BRE can emulate four liquid and solid fuel pool fires to a reasonable extent of producing similar flames and nearly the same fuel properties.

Data have now been examined for 5 s microgravity combustion tests. Two fuels were used, with burning rates of 3–12 g/m^2 s, oxygen mole fractions of 21–30%, and pressures of 0.5–1 bar. The measurements yield the net flame heat flux to the surface and the flame shape. The flame shape is spherical-like and continues to grow roughly linearly with time. However, in some cases the growth appears to be slowing. Apparent local extinction is observed in some cases, particularly when the initial soot breaks through the flame sheet. On the other hand, the net heat flux generally approaches an asymptote after about 3 s, and the center and 8.25 mm locations range from about 2–14 kW/m^2, with the latter location being about 20% higher than the center. A quasi-steady assumption can be made for the state of the system just before the end of the microgravity period. This yields effective heats of gasification associated with condensed-phase fuels.

A steady one-dimensional model allows the data to be correlated. The theory gives good results if $8/\pi$ is increased by 1.5. Two parameters are investigated: the net heat flux, and the length of the flame. The net heat flux is directly related to the burning rate per unit area, and thus it can be concluded that this burning rate is inversely dependent on the diameter of the fuel surface and is a function of the ratio of the ambient oxygen mass fraction and the heat of gasification. The flame length to diameter ratio depends on two dimensionless parameters: B and $Y_{ox,\infty}\Delta h_{c,ox}/Y_{F,o}\Delta h_c$.

Ultimately the BRE is intended to map out a domain of steady burning in microgravity. Table 2 gives an indication of anticipated microgravity flammability for a 25 mm flat fuel with properties ranging from 20 to 40 kJ/g for a heat of combustion, and 0.6–4 kJ/g for a heat of gasification. These property ranges are in the spectrum of solid and liquid fuels, and therefore suggest how such fuels might burn in microgravity. Longer duration tests should yield more complete results.

For a given set of fuel properties, the present data indicates pressure is not a significant variable for burning.

Acknowledgments

We are indebted to invaluable support from NASA, namely technical input from Paul V. Ferkul and Fumiaki Takahashi, and Jay Owens and the microgravity tests directed by Eric Neumann. This study was supported by NASA grant NNX10AD98G.

References

[1] H.D. Ross, Microgravity Combustion, Academic Press, San Diego, 2001.
[2] G. Paczko, N. Peters, K. Seshadri, F.A. Williams, Combust. Theor. Model. 18 (2014) 515–531.
[3] I.S. Wichman, S.L. Olson, F.J. Miller, S.A. Tanaya, Fire Mater. 37 (2013) 503–519.
[4] T.I. Farouk, F.L. Dryer, Combust. Flame 161 (2014) 565–581.
[5] K.L. Pan, M.C. Chiu, Fuel 113 (2013) 757–765.
[6] S. Takahashi, H. Ito, Y. Nakamura, O. Fujita, Combust. Flame 160 (2013) 1900–1902.
[7] J.H. Kimzey, 1974. Skylab Results: Proceedings of the 3rd Space Processing Symposium, vol. 1, NASA TM-X-70752: Marshall Space Flight Center, pp. 115–130.
[8] P.B. Sunderland, B.J. Mendelson, Z.-G. Yuan, D.L. Urban, Combust. Flame 116 (1999) (1999) 376–386.
[9] L. Brahmi, T. Vietoris, S. Rouvreau, P. Joulain, L. David, J.L. Torero, AIAA J. 43 (2005) 1725–1733.
[10] NASA Marshall Space Flight Center, NASA STD-6001, 1998.
[11] T.J. Ohlemiller, An Assessment of the NASA Flammability Screening Test and Related Aspects of Material Flammability, NISTIR 4882, NASA CR-189226, 1992.
[12] Y. Zhang, M.J. Bustamante, M.J. Gollner, P.B. Sunderland, J.G. Quintiere, J. Fire Sci. 32 (2014) 52–71.
[13] L. Orloff, J. de Ris, Proc. Combust. Inst. 13 (1971) 979–992.
[14] J.S. Kim, J. de Ris, W.F. Kroesser, Proc. Combust. Inst. 13 (1971) 949–961.
[15] J. de Ris, L. Orloff, Proc. Combust. Inst. 15 (1975) 175–182.
[16] J.G. Quintiere, Fundamentals of Fire Phenomena, John Wiley & Sons Ltd., Chichester, U.K., 2006.
[17] A. Tewarson, The SFPE Handbook of Fire Protection Engineering, third ed., National Fire Protection Association, Quincy, MA 02269, 2002, pp. 3–82.
[18] L. Li, P.B. Sunderland, Combust. Sci. Technol. 184 (2012) 829–841.
[19] K. Akita, Yumoto, Proc. Combust. Inst. 10 (1965) 943–948.
[20] D.B. Splading, Convective Mass Transfer, McGraw-Hill Book Co., New York, 1963, pp. 23–42.
[21] M. Zarzecki, J.G. Quintiere, R.E. Lyon, T. Rossmann, F.J. Diez, Combust. Flame 160 (2013) 1519–1530.
[22] H.S. Carslaw, J.C. Jaeger, Conduction of Heat in Solids, second ed., Oxford University Press, London, 1959, p. 215.